Experimental simulations of cosmic impacts on rubrene nanoparticles in the water environment reveal the potentiality of condensed phases of polycyclic aromatic hydrocarbons to generate prebiotic molecules

Mara Murri [a,1,*], Alberto Bossi [b], Teresa Recca [c], Marcello Campione [a,*]

[a] Department of Earth and Environmental Sciences, University of Milano-Bicocca, 20126 Milano, Italy
[b] Istituto di Scienze e Tecnologie Chimiche "Giulio Natta" Consiglio Nazionale delle Ricerche (CNR-SCITEC), via G. Fantoli 16/15, 20138 Milano, Italy
[c] Centro Grandi Strumenti, University of Pavia, 27100 Pavia, Italy

ABSTRACT

Organic compounds, such as the polycyclic aromatic hydrocarbons (PAHs), are among the major species responsible for the infrared spectral features characterising the cosmic background radiation. Similar to silicate dust, aggregates rich in carbon with micro- and nano-meter sizes are subjected to several weathering processes in various astrophysical environments that modify their chemistry and structure, thus contributing to the chemical richness of the cosmic environment. In particular, the study of the chemical and structural evolution of PAHs aggregates in the presence of water is relevant to understand the mechanism of formation of the prebiotic building blocks of life.

Pulsed laser ablation of a water-dispersed nano-phase of rubrene (5,6,11,12-tetraphenyltetracene) is here performed to reproduce the high energy-density conditions occurring in shock events in the interstellar medium, while ensuring the presence of a water environment. We studied the structural and chemical evolution of the dispersed rubrene nanocrystals upon laser treatment, showing that rubrene undergoes a fragmentation process producing water soluble species. The results obtained demonstrate that the extreme conditions occurring in cosmic environments coupled with the presence of water are sufficient conditions for transforming PAHs into prebiotic molecules.

1. Introduction

Polycyclic aromatic hydrocarbons (PAHs) are ubiquitous organic molecules populating the interstellar medium and they are the major species responsible of interstellar infrared spectral features (Allamandola et al., 1989; Hrodmarsson et al., 2023; Tielens, 2008). PAHs are also found among the main constituents of carbonaceous chondrites (Elsila et al., 2005; Kalpana et al., 2021; Lecasble et al., 2023; Sabbah et al., 2017).Carbon-rich micrometer and submicrometer-sized aggregates occur in different astrophysical environments and once incorporated into planetary bodies such as asteroids and comets, they can be exposed to meteorites bombardment, grain-grain collisions and similar weathering processes such as those affecting the silicate dust (Kopacz et al., 2023). These processes change the chemistry and structure of the original materials, giving rise to new chemical species which contribute to the chemical richness of the cosmic environment (Fazio et al., 2018; Mimura, 1995; Murri et al., 2022; Thompson et al., 2020). Molecular fragmentation of PAHs is a common relaxation behaviour, together with the emission of IR radiation, after their excitation process due to exposure to high energy photons as occurs in the so-called *photodissociation regions* of molecular clouds (Andrews et al., 2016). The study of the chemical and structural evolution of aggregates of PAHs subjected to extreme conditions is relevant for examining in depth the origin of the densest phases of carbon (e.g., *pre-solar* grains, Davis (2011); Saslaw and Gaustad (1969)) as that of prebiotic building blocks of life (Giese et al., 2022). For this purpose, a lot of effort has been made by the whole scientific community to reproduce in laboratory the planetary conditions responsible for the processing of cosmic dust. In this framework, high-energy pulsed lasers represent consolidated tools for reproducing energy-density conditions similar to those occurring during shock events

* Corresponding authors.
   E-mail addresses: mara.murri@unipv.it (M. Murri), marcello.campione@unimib.it (M. Campione).
[1] Present Address: Department of Earth and Environmental Sciences, University of Pavia, 27100 Pavia, Italy.

in the interstellar medium or micrometeorite impacts on planetary surfaces. Liquid-phase pulsed laser ablation (LP-PLA) is a technique in which high-energy laser pulses are focused on the surface of a solid target immersed in a liquid to induce the ignition of a plasma plume and, consequently, the ablation of the target material and its recondensation in the surrounding liquid in the form of suspended nanoparticles. The presence of the liquid increases to a great extent the pressure achieved at the solid/liquid interface and allows the onset of cooling rates of the order of 10^5 K s^{-1}, likewise to what occurs in circumstellar environments (Kanitz et al., 2019; Patil et al., 1987). Using this technique, nanodiamonds and other carbon allotropes are commonly produced from graphite targets in water or organic liquids (Amans et al., 2017; Cataldo et al., 2018; Marabotti et al., 2022). LP-PLA has been already proven to be a unique and successful technique to synthesize a large variety of nanomaterials and nanoparticles for engineering and medical purposes (Ermakov et al., 2017; Kanitz et al., 2019). Moreover, in the last decades, its application has been extended in several other disciplines and fields such as the planetary sciences, to reproduce space weathering processes in laboratory. These experiments are usually performed on nano dispersions or using a solid target immersed in water (Murri et al., 2022; Thomas et al., 2021).

In this paper, we report the results of the high-energy laser processing in water of a pure nano-phase of rubrene (5,6,11,12-tetraphenyltetracene, see inset in Fig. 1), a PAH constituted by a linear backbone of four condensed benzene rings (like tetracene) with four additional peripheral phenyl groups. The choice of rubrene is motivated by the possibility to obtain commercially available batches of purity higher than 99.9%, and the in-depth knowledge of the photophysical and photochemical properties of both the isolated molecule and molecular aggregates (Braga et al., 2008; Campione, 2008; Ly et al., 2018; Tavazzi et al., 2007). All these characteristics make rubrene an ideal model system to study the evolution of PAHs in response to high-energy processing.

We performed LP-PLA on rubrene nano-phase dispersed in water (i) to simulate space weathering by high-velocity dust impacts and grain-grain collisions in a water environment and (ii) to study its chemical and structural evolution. The water environment aims at simulating conditions that may occur on volatile-rich bodies and those characterized by the presence of hydrous minerals (i.e. phyllosilicates) such as carbonaceous chondrites, dwarf planet Ceres, dark asteroids and also planetary bodies of the outer Solar System (Pieters and Noble, 2016).We monitored the transformation of rubrene nanocrystals under the bombardment of laser pulses by optical spectroscopy and high-resolution transmission electron microscopy (the workflow and the adopted techniques have been summarised in Fig. S1).The analysis of the new water soluble organic fragments, originating from the laser processing simulating cosmic dust impacts, was performed by means of high performance liquid chromatography-mass spectroscopy followed by nuclear magnetic resonance analyses. These results allowed us i) to infer the fragmentation mechanism of the molecules and the water-mediated reactions in which fragments are involved and ii) to demonstrate that the extreme conditions occurring in cosmic environments coupled with the presence of water are sufficient conditions for transforming PAHs into prebiotic molecules.

2. Materials and methods

2.1. Preparation of colloidal solutions of rubrene

Reference colloidal solutions of rubrene in ultrapure water (type I grade) were prepared by the following procedure: 6 ml of absolute ethanol were used to dissolve about 8 mg of rubrene crystalline powder (Rubrene 99.99%, sigma-Aldrich). The resulting solution was sonicated for 5 min and then was left to rest for 10 min in the dark. Then, about 1.5 ml of this solution was added dropwise to 8 ml of water while sonicating for 10 min. The mixing with water induced the precipitation of

nanoparticles of aggregated rubrene molecules that remained suspended forming a colloidal solution

Since it is known that rubrene can crystallize at least in three known polymorphs: monoclinic, orthorhombic and triclinic (Bergantin and Moret, 2012; Huang et al., 2010; Zeis et al., 2006), we performed X-ray diffraction analyses to determine the crystal structure of our colloidal solution. The entire volume of the reference colloidal solution was dried to perform the structural analysis of the rubrene nanoparticles (the dried material was of the order of μg and deposited as thin film on a silicon plate) by means of powder X-ray diffraction using a PANalytical X'Pert PRO with Cu K$_\alpha$ radiation ($\lambda = 1.54$ Å). On the basis of the most intense diffraction peak in the low theta angles region, the dominant crystal phase in our dried rubrene nanoparticles is the triclinic one, with unit-cell parameters: $a = 7.0196$ Å, $b = 8.5432$ Å, $c = 11.948$ Å, $\alpha = 93.04°$, $\beta = 105.58°$, $\gamma = 96.28°$ (Fig. S2 and inset in Fig. 1).

2.2. Liquid phase pulsed laser treatment

The rubrene dispersion in water was placed in a glass cylinder of 2.5 cm in diameter with the liquid level at about 2.2 cm from the vessel base (inset Fig. 1). LP-PLA was performed in house with a Nd:YAG laser at 1064 nm focused via singlet lens in the middle of the solution (~1 cm level from the bottom) and operating at 5 ns and 25 mJ per pulse with a repetition rate of 15 Hz. The focus length was 15 cm.

We performed laser ablation with the aim to simulate space weathering by high-velocity dust impact. For this purpose, the pulse duration was set at 5 ns, which is comparable to the timescale of dust impacts (Sasaki et al., 2001; Yamada et al., 1999) and an energy of tens of mJ corresponds to the energy a cosmic dust particle of ca. 10 μm size travelling at 100 km s^{-1} can transfer by collision to another body. Since our experimental setup lacks a solid target surface, this energy budget is not transferred by focussing the laser beam on a solid surface, but in the volume of the rubrene colloid. Since at 1064 nm the colloid does not show absorption (Fig. 1), the pulse can travel through the liquid volume without losing energy up to the level at which its intensity reaches the threshold for plasma ignition. Indeed, considering a focused beam of section of about 100 μm in the colloid volume, the total irradiated energy per unit area is 320 J cm^{-2}. In terms of energy deposition rate, we attain 10^{10-11} Wcm^{-2}, where plasma ignition is expected. Under this condition, we realized a simulation of energy transfer process coherent with the timescale of gran-grain impacts in a system constituted by solid nanoparticles dispersed in water.

The ablation was performed in air and its total duration was of about 2 h. The solution was stirred for the whole time and monitored via optical spectroscopy measurements (see sec. 2.3).

After the ablation, 2 μl of solution were deposited on a Cu grid for microscopy characterization (see sec. 2.4), while ca. 5 ml were filtered through 0.2 μm pore cellulose-acetate filters to remove the suspended solid fraction. The filtered solution containing possible soluble species (hereafter "the filtered residue") produced during the ablation was divided into two portions of 2.5 ml each for high performance liquid chromatography (see sec. 2.5 HPLC-MS) and nuclear magnetic resonance analyses, respectively (see sec. 2.6 NMR).

2.3. Optical spectroscopy

Absorption and fluorescence measurements of the rubrene colloidal solutions were carried out before, during (every 30 min) and after the ablation experiments. The analyses have been performed by means of optical fibres and an Ocean HDX-XR spectrometer in the range 200–1100 nm (6.20–1.13 eV) with an optical resolution of 1.10 nm. The fluorescence measurements were performed on both the ethanol solution and the water colloid before laser treatment. The same setup was used to collect the radiation emitted by the plasma plume during the ablation experiment (Fig. S3).

2.4. Transmission electron microscopy

High-resolution transmission electron microscopy (HR-TEM) images were collected on the dried rubrene suspension before and after the ablation process, and on the dried filtered residue after the ablation treatment. The samples were prepared by drop-cast of the solutions onto single layer graphene support film, lacey carbon 300 M Cu grids. The TEM analyses were carried with a JEOL JEM 2100Plus instrument at the Microscopy Platform of the University of Milano - Bicocca, using a LaB_6 source and 200 kV of operating voltage. The instrument is equipped with a 9 MP Gatan Rio CMOS camera for image acquisition. Image processing was carried out using the GATAN Digital Micrograph software.

2.5. High performance liquid chromatography-mass spectroscopy (HPLC-MS)

The analytical techniques used included MS and HPLC-MS, which are broadly used to characterize complex mixtures; HPLC can perform efficient separation of different chemical entities (even traces contaminants) mixed in a sample, while MS spectrometry provides molecular weight data and chemical signatures (Maldaner and Jardim, 2012; Penconi et al., 2019; Zou et al., 2022). HPLC-MS measurements were performed at Istituto di Scienze e Tecnologie Chimiche "Giulio Natta" (CNR-SCITEC) at the University of Milano. These analyses were employed here to investigate the water-soluble chemical species produced by laser ablation of rubrene water colloids.

In this work, tandem HPLC-MS analyses were performed with an Agilent HPLC 1260 Infinity series featuring quaternary pump, column hoven (hold at 40 °C), UV and RID detectors. The instrument was coupled to a Shimadzu LCMS-2020 single quadrupole spectrometer, with a mass range 50-2000 Da and accuracy ±0.1 Da, working in electrospray ionization ESI and DUIS (combined Atmospheric Pressure Chemical Ionization APCI – ESI) mode; ESI mode (negative polarity) proved to be more sensitive for these samples given their polar and ionic nature. The analyses were performed in reverse phase with an acetonitrile-water mobile phase modified with the 0.01% formic acid on a Water-Atlantis C18 column (150×4.6 mm^2 and 3 μm particle size). A 20-min gradient program going from 5 to 100% acetonitrile and a 20-min gradient program going from 60 to 95% acetonitrile were used. One vessel containing 2.5 ml of the filtered residue solution produced during the ablation was used for HPLC-MS analyses. The 2.5 ml were dried and redissolved in 20 μl of type I water. The obtained 20 μl of suspension was then injected to perform the measurements. The MS detector mass/charge (m/z) range was monitored in both positive and negative ionization mode.

2.6. Nuclear magnetic resonance (NMR)

The second vessel containing the remaining 2.5 ml of the filtered residue produced during the ablation (5 ml total) was used for NMR analyses. The 2.5 ml of the solution have been dried and dispersed in 0.5 ml of deuterium oxide (D_2O, 99,9% Sigma-Aldrich) and placed in a NMR tube of 5 mm of diameter to conduct the analyses. The measurements were carried out at the Centro Grandi Strumenti of the University of Pavia using a Bruker Av-NEO 700 MHz spectrometer equipped with a TCI CryoProbe. 1H and COSY spectra have been measured at 298 K. Solvent suppression sequence with presaturation (zgpr), available in the Bruker library, was used. The proton spectrum required one thousand scans to achieve a good signal to noise ratio.

3. Results

3.1. Evolution of the optical behaviour of the rubrene water colloids during laser processing

Fig. 1 shows the evolution of the absorption spectra in the UV-VIS range of rubrene nano-phase dispersed in water as a consequence of the pulsed laser ablation process. The bands at 250 and 300 nm are related to the electronic inter-band p–p* transitions (Wali et al., 2022), while those in the visible range (400–600 nm) correspond to the
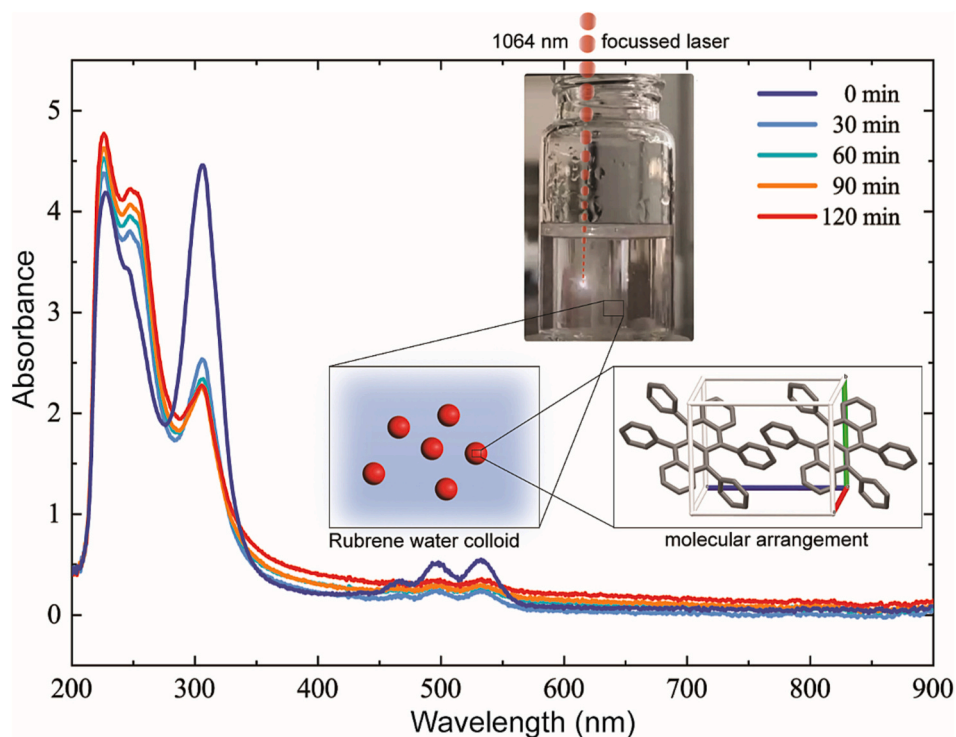
Fig. 1. Optical absorption spectra of rubrene nano-phase dispersed in water for different LP-PLA process times. The inset shows a picture of the flask containing the stirred rubrene water colloid before (0 min) and during laser bombardment with formation of the ablation plume at the laser focal point (top), and the arrangement of rubrene molecules in the dispersed nanoparticles (bottom-right).

vibronic bands related to the ^1L_a-^1A transition (Dutta et al., 1996; Zeng et al., 2007). It is evident how the peak around 300 nm together with those in the visible range (400–600 nm) decrease in intensity as a function of the ablation process.

In contrast, the band at 250 nm increases in intensity, indicating formation of ablation products with lower degree of π-conjugation compared to rubrene.

A similar *bleaching* behaviour is observed after a few hours under ambient conditions (i.e. exposure to air and light, Fig. S4) and attributed to the photo-oxidation of rubrene to rubrene endoperoxide (Ly et al., 2018; Uttiya et al., 2012). However, this optical behaviour is enhanced and accelerated with the laser treatment.

The combined effects of laser processing and the exposure to water can also be observed in the crystallite morphologies revealed in TEM images. Indeed, before laser processing, solid nanoparticles of the order of a few tens of nanometres in size appear well-defined and with regular shape. After laser processing, strong morphological changes are evident both in the suspended solid and in the dried residue. Indeed, the suspended solid appears as composed by ill-defined aggregates showing a flake-like morphology and the dried residue of the filtered liquid phase appears as a percolation lattice with barely recognisable particle domains (Fig. S5).

The fluorescence spectrum of rubrene solutions in ethanol shows the characteristic band in the range 500–700 nm, in agreement with the fluorescence spectra of rubrene solutions reported by Huang et al. (2010) and Zeng et al. (2007). Whereas, the fluorescence spectrum of rubrene water colloids is similar to that of rubrene aggregates reported by Ma et al. (2013) (Fig. S6).

3.2. Fragmentation pattern of rubrene molecules

3.2.1. HPLC- MS

The MS direct injection of the ablation products revealed the presence of 4 recurrent peaks in the negative panel (anions) corresponding to the following *m/z* weights: 321, 291, 277 and 209, with the first peak being the most intense (Fig. 2). The positive panel (cations) is less indicative and therefore it was not reported.

To verify whether these peaks come from different products, HPLC-MS characterization was employed to separate compounds depending on their retention time with the 60–95% gradient program.

Figure 3 reports the full total ion counting HPLC-MS chromatogram (TIC-, see Fig. 3a) and the extracted MS ones based on the previously reported *m/z* weights (Fig. 3b). MS full range masses spectrum of each peak are reported in Fig. S7.
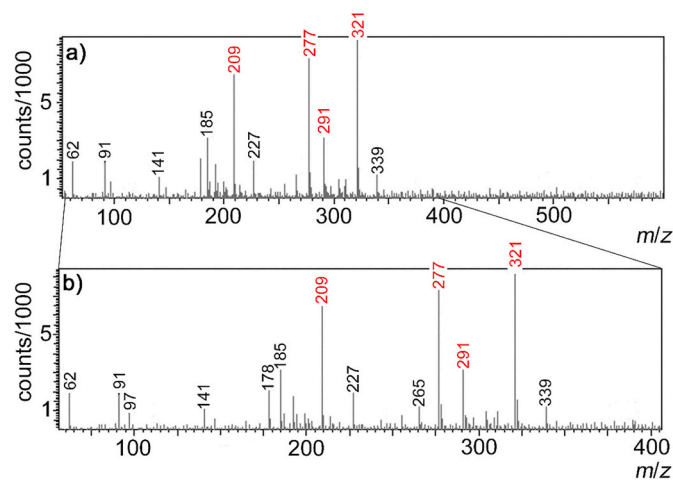
Fig. 2. a) Whole sample full range negative ESI chromatogram and b) the expanded range 50–400 *m/z* of the soluble fraction of ablated rubrene water colloids.
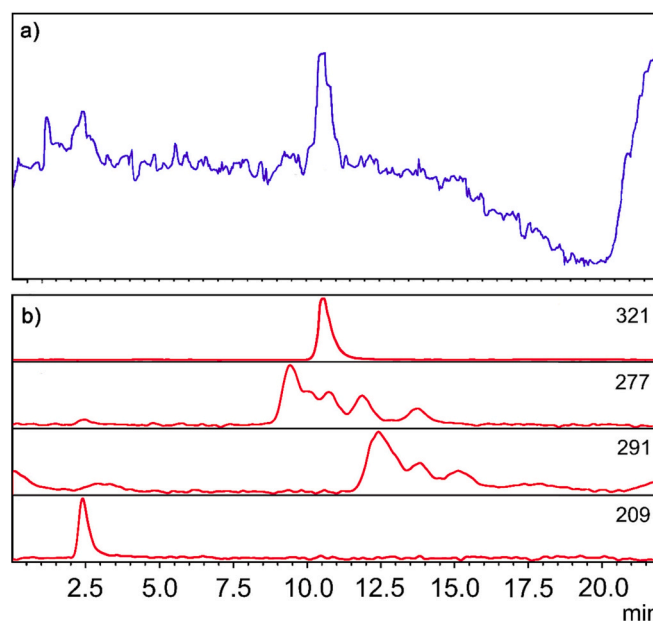
Fig. 3. a) HPLC-MS chromatogram of the soluble fraction of ablated rubrene water colloids and b) the extracted MS chromatograms based on the previously reported *m/z*: 209, 277, 291, 321.

As shown in Fig. 3, the different retention times can be clearly observed from these fragmentation products, indicating their different nature and structures.

These results help understanding the fragmentation pattern of rubrene (molecular weight: 532.69 Da) and allow us to infer the chemical evolution of the starting compound due to exposure to laser processing in the water environment.

3.2.2. Laser-induced fragmentation path of rubrene

Figure 4 shows a tentative path of the laser-induced fragmentation of rubrene colloidal solutions in water on the basis of the results of HPLC-MS (Figs. 2 and 3). Pristine rubrene nanoparticles present a relatively high light absorption cross-section due to their molecular electronic structure (Fig. 1). Hence, rubrene nanoparticles are preferential sites for plasma plume formation and the generation of reactive precursors responsible for the formation of rubrene derivatives. Among these precursors, hydrated electrons play a major role, being a peculiar species forming during high energy-density phenomena occurring in water, able to induce reduction chemical reactions even at sites at a certain distance from that of plume ignition (Broadhead and Tibbets, 2020; Murri et al., 2022). Oxidation reactions are also possible, as a consequence of the high temperature-pressure conditions reached during pulsed laser irradiation in the presence of water. Unlike reduction reaction induced by hydrated electrons, oxidation reaction occurs preferably in proximity of the plasma plume, at the solid particle/liquid interface. Rubrene nanoparticles are molecular aggregates having a cohesion energy of the order of 1 eV per molecule (ca. 10^{-19} J per molecule). This cohesion energy is therefore far lower than that of atomic inorganic crystals, where cohesion energy is of the order of 5 eV per atom. Intramolecular chemical bonds (aromatic C═C bonds) in rubrene have an energy of the order of 500 kJ mol^{-1} (ca. 10^{-18} J per bond). By assuming the volume of the focussed laser pulse to be of the order of 10^{5-6} μm^3 (see sec. 2.2), if entirely occupied by solid rubrene this would involve 10^{-9} mol of rubrene, i.e. 10^{15} molecules. The total cohesion energy of such an ensemble of molecules is of the order of 10^{-4} J, whereas the energy required to fragmentate at the first step (scheme Fig. 4) each molecule within the ensemble is of the order of 10^{-3} J. As can be seen, the laser pulse energy (25 mJ) is sufficient to completely evaporate the nanoparticles present within the excitation volume of the colloid and to
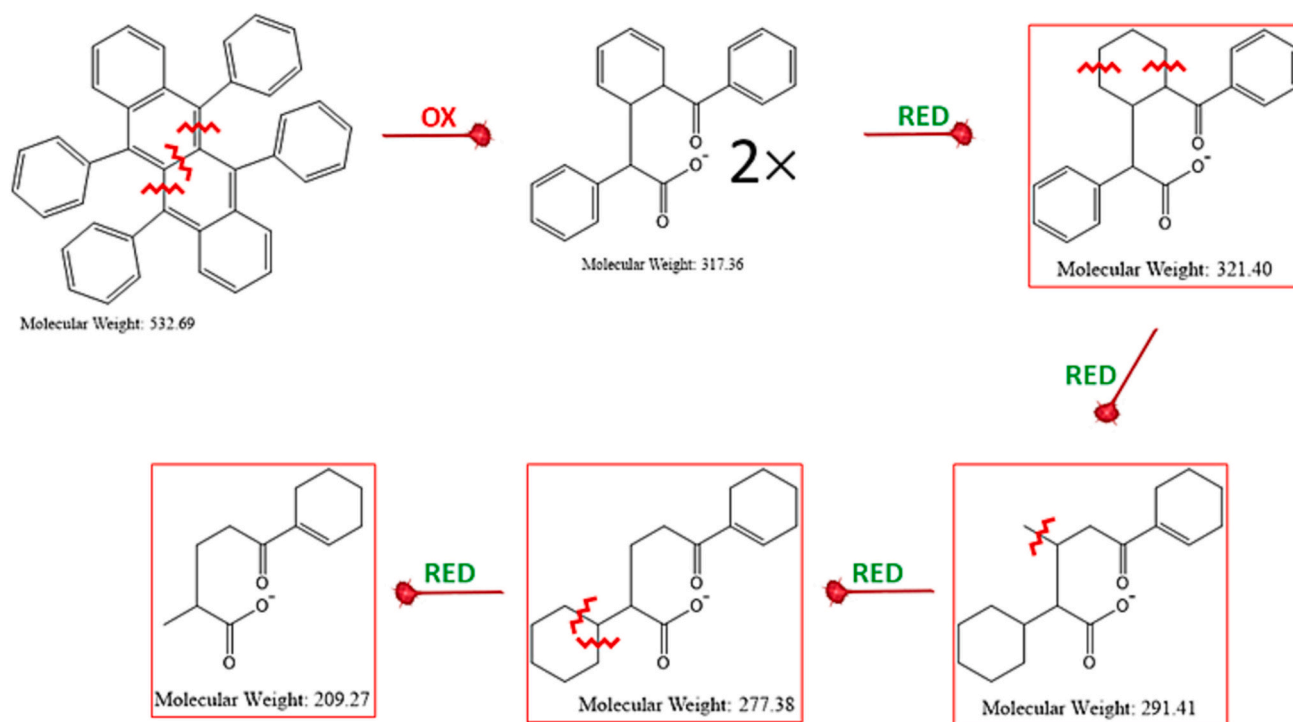
Fig. 4. Fragmentation path of rubrene subjected to irradiation in water by a high-energy pulsed laser, bringing to the soluble anionic molecular moieties detected by mass spectrometry analysis. "OX" indicates a fragmentation accompanied by oxidation reactions, whereas "RED" indicates a fragmentation accompanied by hydrogenation reactions. (For interpretation of the references to colour in this figure legend, the reader is referred to the web version of this article.)

fragmentate the evaporated molecules. Indeed, H- and C-atom emission bands are detected during the ablation experiment, together with O-atom emission band deriving from water, molecular oxygen, or rubrene endoperoxide (Fig. S3).

Under the above considerations, we consider the size of the obtained cluster as irrelevant to the fragmentation dynamics. The important aspect is represented by the possibility to prepare a stable colloid, enabling the clusters to remain suspended during the whole duration of the ablation experiment, creating an extended solid/water interface. This possibility is ensured by the size of clusters, being a few tens of nanometres.

The first fragmentation step consists in the breaking of three consecutive conjugate C—C bonds in the central core of the molecule backbone. This trigger phase is consistent with the fact that intramolecular bonds of this molecular site are relatively less stable, as evidenced by the high propensity of rubrene to add molecular oxygen bridging the 6–11 (or, equivalently, 5–12) C-atoms (Hochstrasser and Ritchie, 1956). The fragmentation process generates C-radicals and subsequent oxidation process generates a ketonic functionality and a carboxylic functionality. The resulting moiety has a molecular weight of 317.36 and, after subsequent hydrogenation of the backbone residual benzylic group, gives rise to a fragment having a weight of 321.40. The important characteristic of this first fragmentation step is the production of two identical molecular moieties. This explains why the 321 fragment is the most recurrent and intense one in mass spectroscopy results.

Subsequent fragmentation bringing to the detected moieties is combined only with hydrogenation reactions, i.e. the formal addition of H-atoms at the C-radicals resulting from the homolytic break of single C—C bonds. Specifically, the 291 fragment is the result of hydrogenation of one entire lateral phenyl ring and a partial hydrogenation of the other lateral phenyl ring, with preservation of a double bond conjugated with the ketonic functionality. C—C bonds break at the residual hexagonal ring of the backbone, with conservation of a methyl group. The 277 fragment results from the breaking of a single C—C bond involving this lateral methyl group of the 291 fragment. Finally, the 209 moiety results

from the fragmentation of the lateral hydrogenated phenyl ring with preservation of a methyl group.

The overall path is characterized by a single initial oxidation event, with successive reductive fragmentations. This is consistent with the localization at the solid/liquid interface of the aforementioned region of laser-induced oxidation (see Murri et al., 2022). Indeed, the oxidation event produces uncoloured soluble fragments which disperse in water. These dilute fragments, due to their reduced conjugation and then reduced absorption cross-section (Fig. 1), are subjected to a less drastic laser processing. However, thanks to the presence of weaker single C—C bonds, these fragments are furtherly broken into smaller moieties while acting as targets of hydrated electrons produced at the solid particle/liquid interface. This induces their further hydrogenation following the path depicted in Fig. 4.

3.3. Chemical analysis of produced fragments by NMR

In order to corroborate the fragmentation pattern comprising the abovementioned compounds, we carried out nuclear magnetic resonance analyses.

The assignment of all signals in the proton spectrum is made difficult by the low concentration of the sample and the presence of a mixture of compounds in solution. However, by matching the acquired 1H spectrum with the predicted ones (NMRSim, Bruker BioSpin, Fig. S8) and with the information from the COSY (Fig. S9), several peaks characteristic of the compounds under consideration were identified.

The obtained 1H spectrum (Fig. 5) is in accordance with the presence of different compounds in the solution. The assignment of the peaks was carried out by comparison of the experimental spectrum against the predicted ones and coupled with the information from the COSY (Fig. S9) (NMR).

The region of the 1H spectrum from 8.2 to 6.4 ppm (Fig. 5a) revealed the presence of aromatic protons as those forming the compound having $m/z = 321$, while the peak near 7 ppm and highlighted in yellow showed the presence of a double bond characteristic of the other three
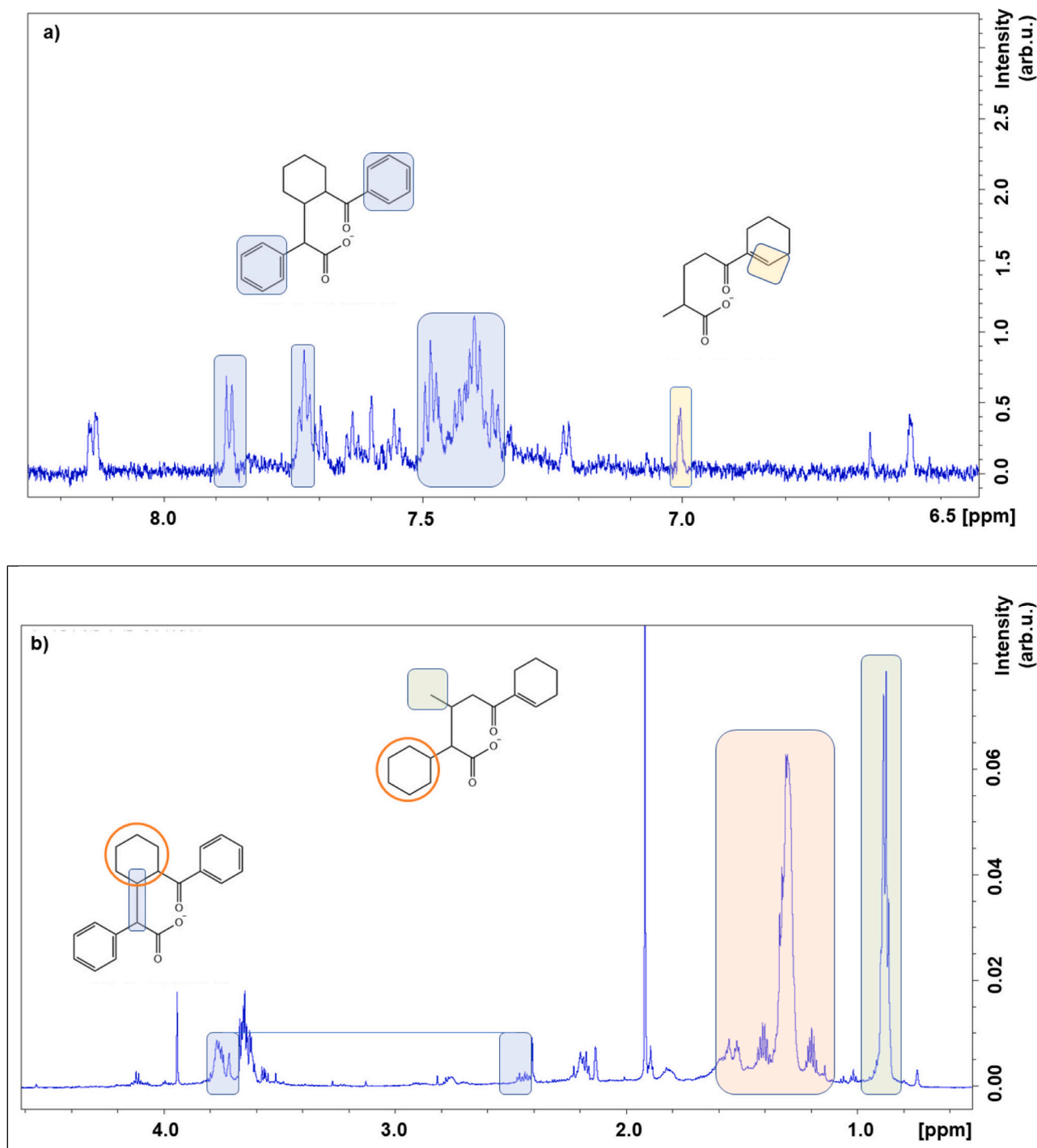
Fig. 5. a) NMR 1H spectrum of the soluble solid fraction of ablated rubrene water colloids dispersed in D_2O, revealing the presence of aromatic and b) aliphatic compounds.

compounds (m/z = 291, 277, and 209, see Fig. 2).

In the aliphatic region, the peak at 0.8 ppm related to the signal of -CH_3 group has been detected and related to the compound with m/z = 291. Signals around 3.8 ppm, which are correlated in the COSY spectrum to those near 2.4 ppm, could be related to the fragment of the aromatic compound (see the region highlighted in blue in Fig. 5b). Whereas, the crowded region from 1 to 2 ppm could point out the presence of -$CH2$- groups related to the aliphatic ring signals.

4. Discussion

PAHs are considered as key precursors for the generation of prebiotic molecules, such as carboxylic acids and amino-acids (Fioroni and DeYonker, 2022). They are detected in various cosmic regions by means of their mid-IR emission bands, however when they enter denser regions they condense onto cold grains and their emissions are quenched. Here, they are exposed to UV-photon irradiation and cosmic impact rays which can drive the nucleation of new other species (Bouwman et al., 2011; Castellanos et al., 2018; Cook et al., 2015; Öberg, 2016; Zhen

et al., 2015).

Hydrothermal alteration was also suggested as a possible transformation mechanism of PAHs into other organic derivatives in carbonaceous chondrites (Lecasble et al., 2023 and references therein). However, the type of chemical reactions involved, together with the new forming molecule or compound, change as a function of the external conditions, and recent extensive studies by Giese et al. (2022) reported that reactions occurring during hydrothermal/aqueous alteration do not produce amino acids, even if their formation is predicted by thermodynamic studies.

In our experiments, the water medium and the laser treatment were used to simulate cosmic environments that experienced aqueous alteration, such as those related to carbonaceous chondrites, (Garenne et al., 2016; Grimm and McSween Jr, 1989) with the aim to explore possible formation mechanisms of prebiotic molecules starting from PAHs.

The *bleaching* behaviour of the colloid during and after the laser treatment, monitored by means of optical absorption measurements, is similar to the one observed by Uttiya et al. (2012) due to photo-oxidation. However, the chemical reactions triggered by the laser treatment are the results of a complexity of events rather than simple transformation into rubrene *endo*-peroxide (which is a non-soluble species, then excluded in our analyses). The sequence of the events and processes acting during laser processing are i) energy deposition into the PAHs aggregate through a rapid process (simulating a cosmic shock event); ii) molecular fragmentation and formation of a plasma plume concentrating a load of C-atoms; iii) reaction of the plasma with water and molecular fragments and condensation of the products in the water environment.

The compounds determined in our experiment, populating the soluble fraction of the initial sample, are carboxylic acids with relatively low molecular weight and some residual aromatic character. These characteristics make them relevant as prebiotic compounds. Their presence is the result of a sequence of both oxidation and reduction (hydrogenation) reactions (Fig. 4) which cannot be reproduced by simple hydrothermal conditions (Andrews et al., 2016; Hrodmarsson et al., 2023). Within this chemical-physical framework, it is noteworthy the absence of a role played by a solid mineral surface. Rather, we consider the shock conditions as a fundamental constraint to enable the rapid transformation of PAHs into prebiotic compounds.

5. Conclusions

We reported the results of experimentally simulated experiments of space weathering of solid nano-aggregates of rubrene dispersed in the water environment. The reproduced shock conditions, thanks to the use of high energy and focused laser pulses directed to the volume of rubrene water colloids, were sufficient to produce soluble carboxylic acids as a result of fragmentation of the pristine molecule and subsequent oxidation/reduction events mediated by the water environment. These results highlight the importance of high energy-density events (cosmic impacts, shocks, etc.) for the generation of prebiotic compounds starting from the ubiquitous PAHs, while mitigating the relevance of hydrothermal alterations catalysed by mineral surfaces. The role played by the water medium is simultaneously enhanced, for two reasons: on the one hand, we showed that it aids both oxidation and reduction reactions, necessary for the formation of complex molecules; on the other hand, while recently the surface of water droplets was demonstrated to aid the otherwise inhibited polymerization of amino acids into peptides (Holden et al., 2022), we provide a possible mechanism for the previous step of formation of prebiotic molecules within the water volume.

Declaration of Competing Interest

The authors declare that there are no conflicts of interest.

Data availability

Data will be made available on request.

Appendix A. Supplementary data

Supplementary data to this article can be found online at https://doi.org/10.1016/j.icarus.2023.115727.

References

Allamandola, L., Tielens, A., Barker, J., 1989. Interstellar polycyclic aromatic hydrocarbons-the infrared emission bands, the excitation/emission mechanism, and the astrophysical implications. Astrophys. J. Suppl. Ser. 71, 733–775.

Amans, D., Diouf, M., Lam, J., Ledoux, G., Dujardin, C., 2017. Origin of the nano-carbon allotropes in pulsed laser ablation in liquids synthesis. J. Colloid Interface Sci. 489, 114–125.

Andrews, H., Candian, A., Tielens, A., 2016. Hydrogenation and dehydrogenation of interstellar PAHs: spectral characteristics and H2 formation. Astron. Astrophys. 595, A23.

Bergantin, S., Moret, M., 2012. Rubrene polymorphs and derivatives: the effect of chemical modification on the crystal structure. Cryst. Growth Des. 12, 6035–6041.

Bouwman, J., Cuppen, H., Steglich, M., Allamandola, L., Linnartz, H., 2011. Photochemistry of polycyclic aromatic hydrocarbons in cosmic water ice-II. Near UV/VIS spectroscopy and ionization rates. Astron. Astrophys. 529, A46.

Braga, D., et al., 2008. Bulk electrical properties of rubrene single crystals: measurements and analysis. Phys. Rev. B 77, 115205.

Broadhead, E.J., Tibbetts, K.M., 2020. Fabrication of Gold–Silicon Nanostructured Surfaces with Reactive Laser Ablation in Liquid. Langmuir. 36, 10120–10129.

Campione, M., 2008. Rubrene heteroepitaxial nanostructures with unique orientation. J. Phys. Chem. C 112, 16178–16181.

Castellanos, P., Candian, A., Zhen, J., Linnartz, H., Tielens, A., 2018. Photoinduced polycyclic aromatic hydrocarbon dehydrogenation the competition between H-and H2-loss. Astron. Astrophys. 616, A166.

Cataldo, F., Ursini, O., Milani, A., Casari, C.S., 2018. One-pot synthesis and characterization of polyynes end-capped by biphenyl groups (α, ω-biphenylpolyynes). Carbon. 126, 232–240.

Cook, A.M., et al., 2015. Photochemistry of polycyclic aromatic hydrocarbons in cosmic water ice: the role of PAH ionization and concentration. Astrophys. J. 799, 14.

Davis, A.M., 2011. Stardust in meteorites. Proc. Natl. Acad. Sci. 108, 19142–19146.

Dutta, A., Misra, T., Pal, A., 1996. Two photon delayed fluorescence emission from aggregates of rubrene in Langmuir-Blodgett films at 77 K. Solid State Commun. 99, 767–771.

Elsila, J.E., de Leon, N.P., Buseck, P.R., Zare, R.N., 2005. Alkylation of polycyclic aromatic hydrocarbons in carbonaceous chondrites. Geochim. Cosmochim. Acta 69, 1349–1357.

Ermakov, V.A., et al., 2017. Size control of silver-core/silica-shell nanoparticles fabricated by laser-ablation-assisted chemical reduction. Langmuir. 33, 2257–2262.

Fazio, A., Harries, D., Matthäus, G., Mutschke, H., Nolte, S., Langenhorst, F., 2018. Femtosecond laser irradiation of olivine single crystals: experimental simulation of space weathering. Icarus 299, 240–252.

Fioroni, M., DeYonker, N.J., 2022. Nitrile regio-synthesis by Ni centers on a siliceous surface: implications in prebiotic chemistry. Chem. Commun. 58, 11579–11582.

Garenne, A., et al., 2016. Bidirectional reflectance spectroscopy of carbonaceous chondrites: implications for water quantification and primary composition. Icarus. 264, 172–183.

Giese, C.-C., et al., 2022. Experimental and theoretical constraints on amino acid formation from PAHs in Asteroidal settings. ACS Earth Space Chem. 6, 468–481.

Grimm, R.E., McSween Jr., H.Y., 1989. Water and the thermal evolution of carbonaceous chondrite parent bodies. Icarus. 82, 244–280.

Hochstrasser, R.M., Ritchie, M., 1956. The photoformation and thermal decomposition of rubrene peroxide. Trans. Faraday Soc. 52, 1363–1373.

Holden, D.T., Morato, N.M., Cooks, R.G., 2022. Aqueous microdroplets enable abiotic synthesis and chain extension of unique peptide isomers from free amino acids. Proc. Natl. Acad. Sci. 119, e2212642119.

Hrodmarsson, H.R., Bouwman, J., Tielens, A.G., Linnartz, H., 2023. Fragmentation of the PAH cations of Isoviolanthrene and Dicoronylene: a case made for interstellar cyclo [n] carbons as products of universal fragmentation processes. Int. J. Mass Spectrom. 485, 116996.

Huang, L., Liao, Q., Shi, Q., Fu, H., Ma, J., Yao, J., 2010. Rubrene micro-crystals from solution routes: their crystallography, morphology and optical properties. J. Mater. Chem. 20, 159–166.

Kalpana, M., Babu, E., Mani, D., Tripathi, R., Bhandari, N., 2021. Polycyclic aromatic hydrocarbons in the Mukundpura (CM2) chondrite. Planet. Space Sci. 198, 105177.

Kanitz, A., Kalus, M., Gurevich, E., Ostendorf, A., Barcikowski, S., Amans, D., 2019. Review on experimental and theoretical investigations of the early stage, femtoseconds to microseconds processes during laser ablation in liquid-phase for the synthesis of colloidal nanoparticles. Plasma Sources Sci. Technol. 28, 103001.

Kopacz, N., et al., 2023. The photochemical evolution of polycyclic aromatic hydrocarbons and nontronite clay on early earth and Mars. Icarus. 115437.

Lecasble, M., Bernard, S., Viennet, J.-C., Criouet, I., Remusat, L., 2023. Influence of hydrothermal asteroidal conditions on the molecular structure and isotopic compositions of polycyclic aromatic hydrocarbons. Icarus. 401, 115603.

Ly, J.T., et al., 2018. Oxidation of rubrene, and implications for device stability. J. Mater. Chem. C 6, 3757–3761.

Ma, L., et al., 2013. Fluorescence from rubrene single crystals: interplay of singlet fission and energy trapping. Phys. Rev. B 87, 201203.

Maldaner, L., Jardim, I.C., 2012. Determination of some organic contaminants in water samples by solid-phase extraction and liquid chromatography–tandem mass spectrometry. Talanta. 100, 38–44.

Marabotti, P., et al., 2022. In situ surface-enhanced Raman spectroscopy to investigate polyyne formation during pulsed laser ablation in liquid. Carbon. 189, 219–229.

Mimura, K., 1995. Synthesis of polycyclic aromatic hydrocarbons from benzene by impact shock: its reaction mechanism and cosmochemical significance. Geochim. Cosmochim. Acta 59, 579–591.

Murri, M., et al., 2022. Laboratory simulation of space weathering on silicate surfaces in the water environment. ACS Earth Space Chem. 6, 197–206.

Öberg, K.I., 2016. Photochemistry and astrochemistry: photochemical pathways to interstellar complex organic molecules. Chem. Rev. 116, 9631–9663.

Patil, P., et al., 1987. Pulsed-laser–induced reactive quenching at liquid-solid interface: aqueous oxidation of iron. Phys. Rev. Lett. 58, 238.

Penconi, M., et al., 2019. Unraveling the degradation mechanism in firpic-based blue OLEDs: II. Trap and detect molecules at the interfaces. Chem. Mater. 31, 2277–2285.

Pieters, C.M., Noble, S.K., 2016. Space weathering on airless bodies. J. Geophys. Res.: Planets. 121, 1865–1884.

Sabbah, H., Bonnamy, A., Papanastasiou, D., Cernicharo, J., Martín-Gago, J.-A., Joblin, C., 2017. Identification of PAH isomeric structure in cosmic dust analogs: the AROMA setup. Astrophys. J. 843, 34.

Sasaki, S., Nakamura, K., Hamabe, Y., Kurahashi, E., Hiroi, T., 2001. Production of iron nanoparticles by laser irradiation in a simulation of lunar-like space weathering. Nature. 410, 555–557.

Saslaw, W.C., Gaustad, J.E., 1969. Interstellar dust and diamonds. Nature. 221, 160–162.

Tavazzi, S., et al., 2007. Optical response and emission waveguiding in rubrene crystals. Phys. Rev. B 75, 245416.

Thomas, A., Parvathy, M., Jinesh, K., 2021. Synthesis of nanodiamonds using liquid-phase laser ablation of graphene and its application in resistive random access memory. Carbon Trends. 3, 100023.

Thompson, M., et al., 2020. The effect of progressive space weathering on the organic and inorganic components of a carbonaceous chondrite. Icarus. 346, 113775.

Tielens, A.G., 2008. Interstellar polycyclic aromatic hydrocarbon molecules. Annu. Rev. Astron. Astrophys. 46, 289–337.

Uttiya, S., et al., 2012. Stability to photo-oxidation of rubrene and fluorine-substituted rubrene. Synth. Met. 161, 2603–2606.

Wali, S., et al., 2022. Organic rubrene/topological insulator bi 2 se 3/SiO 2 hybrid heterojunction photodetectors for broadband and ultrafast photodetection application. J. Mater. Chem. C 10, 1289–1301.

Yamada, M., et al., 1999. Simulation of space weathering of planet-forming materials: nanosecond pulse laser irradiation and proton implantation on olivine and pyroxene samples. Earth, Planets Space. 51, 1255–1265.

Zeis, R., Besnard, C., Siegrist, T., Schlockermann, C., Chi, X., Kloc, C., 2006. Field effect studies on rubrene and impurities of rubrene. Chem. Mater. 18, 244–248.

Zeng, X., Zhang, D., Duan, L., Wang, L., Dong, G., Qiu, Y., 2007. Morphology and fluorescence spectra of rubrene single crystals grown by physical vapor transport. Appl. Surf. Sci. 253, 6047–6051.

Zhen, J., et al., 2015. Laboratory photo-chemistry of PAHs: ionization versus fragmentation. Astrophys J. Lett. 804, L7.

Zou, J., Yao, B., Yan, S., Song, W., 2022. Determination of trace organic contaminants by a novel mixed-mode online solid-phase extraction coupled to liquid chromatography–tandem mass spectrometry. Environ. Pollut. 303, 119112.